

Supporting information

Controlled synthesis of Ru-single-atoms on ordered mesoporous phosphine polymer for microwave-assisted conversion of biomass-derived sugars to artificial sweeteners

Arindam Modak,* Deepika Gill, Akshay R. Mankar, Kamal K. Pant*, Vidha Bhasin, Chandrani Nayak, Saswata Bhattacharya*

***Correspondance to:**

A. Modak (arindam_modak_2006@yahoo.co.in)

K.K. Pant (kkpant@chemical.iitd.ac.in)

S. Bhattacharya (saswata@physics.iitd.ac.in)

Experimental section

Methods

Chemicals and reagents. Catechol (Cat), benzene, triphenylphosphine (PPh), triphenylamine (Am), 1,2-dichloroethane (DCE), dimethoxymethane (DMM), hexadecyltrimethylammonium bromide, ammonia solution (28% in water), n-hexane, and all other solvents were obtained from Merck and used as received. Hydrated ruthenium salt ($\text{RuCl}_3 \cdot x\text{H}_2\text{O}$), tetraethyl orthosilicate, LUDOX® HS-40 colloidal silica (40 wt. % suspension in water) were procured from Sigma-Aldrich, USA for the synthesis of catalysts. D-(+)-xylose 99%, D-(+)-glucose >99.5%, xylitol >99%, D-sorbitol 99% from Sigma-Aldrich, USA were used for the preparation of standards of several concentrations and getting the calibration curve. Formic acid, 97% and triethylamine, 99% were received from Alfa Aesar. HPLC grade water was used for all the reactions as well as in the mobile phase (5 mM sulphuric acid) of HPLC operation.

Instrumentation. Nitrogen adsorption-desorption isotherm and pore size distribution of the catalysts are measured at $-196\text{ }^\circ\text{C}$ using Quantachrome Instruments Autosorb 1C surface area analyzer. For such analysis, samples are degassed at $150\text{ }^\circ\text{C}$ for 4 h. Pore size analysis was obtained considering the density functional theory (DFT) model approach using N_2 at 77 K on carbon at cylindrical pores. Stability of the samples was measured from Thermogravimetric analysis using NETZSCH STA 449F3 analyzer within the temperature ranges $25\text{-}800\text{ }^\circ\text{C}$ at a heating rate of $10\text{ }^\circ\text{C min}^{-1}$ in air. X-ray photoelectron spectroscopy (XPS) was recorded by VG ESCALAB MK2, using $\text{AlK}\alpha$ ($h\nu = 1486.6\text{ eV}$) as the excitation source. Fourier transform infrared spectra (FT-IR) were measured on a Nicolet Nexus 470 IR spectrometer. Ru content in the catalysts was obtained using microwave plasma atomic emission spectroscopy (MPAES, Agilent, 4210). Wide-angle X-ray diffractions were

obtained from $2\theta \sim 5-90^\circ$ at 5° min^{-1} scan speed using X'Pert PRO (PANalytical Netherlands). Small-angle X-ray scattering of the catalysts was measured from Bruker D8 Advance X-ray diffractometer fitted with Ni-filtered Cu $K\alpha$ radiation source of wavelength 0.15406 nm. Morphology of the particles was found from FESEM-EDX (JEOL JMS-7800F prime) and the samples were prepared by dipping them on a carbon tap. Microstructure analysis (TEM and HRTEM images) of the catalysts were taken from HITACHI HT7700 at an acceleration voltage of 100 kV. Before HRTEM, 1-2 mg sample was dispersed in 4 mL ethanol (99.8%, Sigma Aldrich) through 4-5 min sonication and then drop cast on the Cu grid. Carbon, hydrogen, and nitrogen contents were determined using a Perkin Elmer 2400 Series II CHN analyzer. Aberration-corrected HAADF-STEM images are recorded by a JEOL-FEG JEMF200 high-resolution transmission electron microscope operating at 200 kV. XPS analysis was done using Model/Supplier: PHI 5000 Versa Prob II, FEI Inc. *In-situ* CO adsorption was measured by Thermo Fisher IS50 FTIR HARRICK DRIFT setup. Initially, the catalysts were treated under CO flowing for 30 min, followed by purging with N_2 to collect spectrum at 25°C . Solid-state magic angle ^{31}P NMR has carried out with Varian Infinity Plus 400 spectrometer with 161.8 MHz frequency using $(\text{NH}_4)_2\text{HPO}_4$ as reference. Extended X-ray Absorption Fine Structure (EXAFS) measurements have been carried out at the Energy-Scanning EXAFS beamline (BL-9) at the Indus-2 Synchrotron Source (2.5 GeV, 100 mA) at Raja Ramanna Centre for Advanced Technology (RRCAT), Indore, India (See SI for details).

Preparation of phosphine containing porous ligand (PPh). Benzene (0.4 g), dimethoxymethane (1.2 g), and triphenylphosphine (0.655 g) were mixed together in 1,2-dichloroethane (20 mL) with stirring under N_2 atmosphere. Then the solution was ice-cooled and anhydrous FeCl_3 (2.4 g) was gradually (portion-by-portion) added to the solution. After

half an hour, the reaction mixture was moved to an oil bath and heated at 80 °C for 24 h under N₂ and finally cooled to 25 °C and added methanol. The precipitate was rigorously washed with methanol and water until the filtrate shows colorless. A laborious washing of the porous ligand was continued for 48 h using Soxhlet Apparatus with methanol as solvent. Dark brownish yellow product was recovered after 24 h drying in an oven at 70 °C. The porous ligand was named as PPh.

Synthesis of Ru-PPh. 0.2 g PPh ligand was dispersed in a round bottom flask containing 5 mL water to make a slurry. Then 20 mg RuCl₃.xH₂O (10 wt.% to polymer) was added and it was refluxed at 80 °C under N₂ atmosphere for 24 h. The mixture was then centrifuged and washed thoroughly with water until the solution shows colorless. The brownish catalyst was dried in an oven at 60 °C prior to reactions. Ru loading was investigated through ICP analysis and found as 1 wt.%.

Modification of catalysts. To show the electronic effect on Ru, other additional ligands based on catechol and triphenylamine moiety were used for the preparation of the porous amine and catechol-based ligands.

Preparation of ruthenium-catechol-based porous ligand (Ru-Cat). The Catechol-based porous ligand was synthesized according to the previous method after slight modification¹. Briefly, 1 g catechol was dissolved in 20 mL dichloroethane by vigorous stirring. Then 1.38 g dimethoxymethane was slowly added with continuous stirring. Later, 1.46 g anhydrous FeCl₃ was gradually added through stirring for 1 h and then heated to 80 °C for 24 h under N₂. The Final product was collected by filtration and purification through a rigorous soxhlet extraction process using methanol as solvent. The dried catechol-based POP was used for

loading ruthenium, following the exactly similar process as described before. Ru loading was 1.1 wt%, based on ICP analysis.

Preparation of ruthenium-based triphenylamine containing porous ligand (Ru-AmPh).

Benzene (0.4 g), dimethoxymethane (1.17 g), triphenylphosphine (0.655 g), triphenylamine (0.3 g) were dissolved in 20 mL dichloroethane and stirred under N₂ atmosphere. It was cooled in ice water (0 °C) and then anhydrous FeCl₃ (2.5 g) was gradually added portion by portion, and heated at 80 °C for 24 h using an oil bath under N₂ atmosphere. The Final product was collected by filtration, and rigorous washing using soxhlet extraction with methanol until the filtrate shows colorless. The air-dried product was used for loading ruthenium following similar methods. It shows Ru loading of 1 wt.% through ICP analysis.

Synthesis of silica templates. SBA-15 was prepared according to the literature procedure as mentioned elsewhere². Cubic mesoporous silica (MesoSi) was prepared by modifying the previously reported synthesis³. Typically, 2 g cetyltrimethylammonium bromide (CTAB) was dissolved in 160 mL distilled water under slow stirring. Then, 14 mL NH₃ solution (28 wt.%) was added dropwise to the CTAB solution to make it clear and transparent. Next, a mixture of hexane (40 mL) and TEOS (10 mL) was added very slowly to the solution to complete the addition within 60 min through continuous stirring at 40 °C. As the reaction continues, a milky white colloidal solution was formed which was centrifuged and separated, washed with deionized water and ethanol. CTAB template was carefully removed from the collected solid through solvent extraction at 80 °C using a mixture of ethanol and 2 M HCl. The extraction method was repeated five times until it shows ~60% weight loss as compared to the as-prepared MesoSi. Eventually, MesoSi was centrifuged and air-dried.

Synthesis of silica/polymer composite. We used SBA-15 and MesoSi as hard templating sources to make the composite catalysts. To synthesize the composite, initially, 0.2 g SBA-15 or MesoSi was dispersed in 20 mL dichloroethane in a round bottom flask followed by the addition of polymerization precursors and refluxing at 80 °C for 24 h under N₂. The dark brown color composite was isolated by filtration and the washing was repeated several times (thrice) to remove unreacted monomers and additional impurities. Final purification was accomplished by the soxhlet extraction method using methanol as solvent.

Template-free preparation of the ordered polymers. Silica template was carefully removed from the composite nanostructures⁴. To remove silica from the composite, we used an HF solution (48%). Initially, the composite materials were dispersed in water (10 mL) in a polypropylene flask and then 10 mL HF (48%) was added very carefully into the solution. The solution was kept for stirring at 25 °C for 6 to 12 h to monitor the removal effect of silica through TGA analysis. The as-prepared materials after modification with SBA-15, MesoSi, and colloidal silica as templates are named as PPh-SBA and , PPh-MesoSi respectively.

Preparation of Ru-loaded ordered polymers. 0.2 g template-free porous polymers were dispersed in a round bottom flask in 5 mL water along with 20 mg RuCl₃.xH₂O to make a slurry. The resulting slurry was refluxed at 80 °C under N₂ atmosphere for 20 h. The mixture was collected through centrifugation and extensively washed with water until the solution shows colorless. It was dried in an oven at 70 °C prior to reactions. Final catalysts are denoted as Ru-PPh-SBA, Ru-PPh-MesoSi.

Xylose / Glucose hydrogenation. The hydrogenation reactions were performed in a microwave reactor (Anton Paar: Monowave 300) to produce xylitol via *in-situ* hydrogenation

using formic acid (HCOOH, FA) and triethylamine (TA) mixture. The reactor is equipped with a temperature sensor, pressure sensor, cooling system, magnetic stirring assembly. In a typical reaction, the 10 mL borosilicate glass vial is charged with 20 mg (0.1 mmol) substrates (xylose/glucose), 10 mg Ru-catalysts (1 wt% Ru) and then dispersed in 2 mL ultrapure water (HPLC grade). Further, FA and TA were added (TA:FA = 0.2-1.2 molar ratio), a magnetic bead was placed and the vial was sealed with the silicone septum. The resulting vial containing the solution of the reaction mixture was sonicated for 2 min to disperse the heterogeneous mixture and then placed in the cavity of the microwave reactor at 80-140 °C for the desired time (2 h). After the completion of the reaction time, the vial was cooled to 50 °C using the cooling system provided with the reactor. Finally, the filtrate was collected by centrifugation and analyzed using HPLC. All the reactions were repeated thrice and the average of the results is reported. To obtain the best-optimized condition, T (80-140 °C), time and TA/FA ratio (0.2-1.2) was varied.

Product analysis. The catalyst was separated from the product mixture using centrifugation and the filtrate was passed through a micro-syringe filter before being analyzed by high-performance liquid chromatography (HPLC). HPLC (Agilent 1200 infinity series) equipped with an autosampler, refractive index (RI) detector and Aminex HPX-87H column (300 x 7.8 mm) was used for the quantification of xylose, xylitol, glucose, and sorbitol. The column temperature was maintained at 50 °C. The injection volume of 2 μL , flow rate of 0.6 mL min^{-1} was fixed and sulphuric acid (5 mM) was used as the mobile phase. All the samples were injected thrice and the average readings were used for the calculation of the xylose/glucose conversion, xylitol/sorbitol yield and selectivity on a weight basis, using the following equations (Eq.1-3):

$$\% \text{ Conversion of xylose/glucose} = \frac{\text{Amount of xylose/glucose reacted (mg)}}{\text{initial amount of xylose/glucose fed (mg)}} \times 100 \quad (1)$$

$$\% \text{ Yield of xylitol/sorbitol} = \frac{\text{amount of xylitol/sorbitol produced (mg)}}{\text{initial amount of xylose/glucose fed (mg)}} \times 100 \quad (2)$$

$$\% \text{ Selectivity of xylitol/sorbitol} = \frac{\text{amount of xylitol/sorbitol produced (mg)}}{\text{Amount of xylose/glucose reacted (mg)}} \times 100 \quad (3)$$

Recycling experiments. Ru-PPh-MesoSi was recycled six times. The catalyst was separated by centrifugation and washed thoroughly with water and dried at 80 °C overnight before doing recycling experiments.

Computational details. Density functional theory (DFT) calculations were performed with Projector augmented wave (PAW) Pseudopotential^{5,6} as implemented in Vienna *ab initio* Simulation Package (VASP)^{31,32}. In all the calculations, the generalized gradient approximation (GGA) was used with the Perdew-Burke-Ernzerof (PBE) exchange-correlation functional⁷. We have also validated results using more advanced hybrid functionals (viz. HSE06). For highly-accurate calculations, the cut-off energy of 500 eV was preferred for the plane-wave basis set. The electronic self-consistency was attained with an energy tolerance of 0.001 meV. For obtaining fully relaxed electronic configurations, Hellman-Feynmann forces were converged with a limit of 0.005 eV/Å using conjugate gradient (CG) minimization. The Γ -centered 1x1x1 k-grid sampling is employed for the optimization of electronic configurations. To obtain the partial charges of all the atoms in different electronic configurations the Hirshfeld model was used. The adsorption energy (E_{ad})

of the adsorbate (glucose/xylose) is computed taking the difference of respective ground state energies, i.e.

$$E_{\text{ad}} = E_{\text{catalyst+glucose/xylose}} - E_{\text{glucose/xylose}} - E_{\text{catalyst}} \quad (4)$$

Where, E_{catalyst} , $E_{\text{glucose/xylose}}$, and $E_{\text{catalyst+glucose/xylose}}$ correspond to the total energy of the catalyst (Ru atom surrounded by different ligands), adsorbate (glucose/xylose) and the adsorbate adsorbed on the catalyst. Notably, the more negative is the E_{ad} , more is the adsorption strength. To have a qualitative understanding of the charge distribution, electron density difference analysis is carried out. Electron density difference $\Delta\rho = \rho(\text{Ru-atom} + \text{ligands surrounding Ru}) - \rho(\text{Ru-atom}) - \rho(\text{ligands surrounding Ru})$.

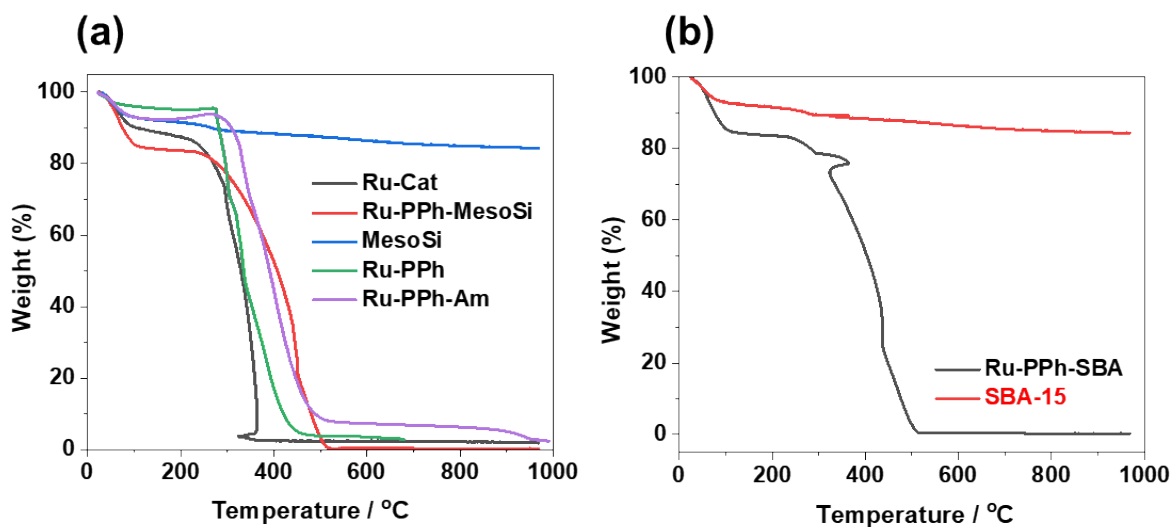


Fig. S1 TGA spectra of (a) Ru-catalysts and (b) template-free silica precursors, performed under air atmosphere

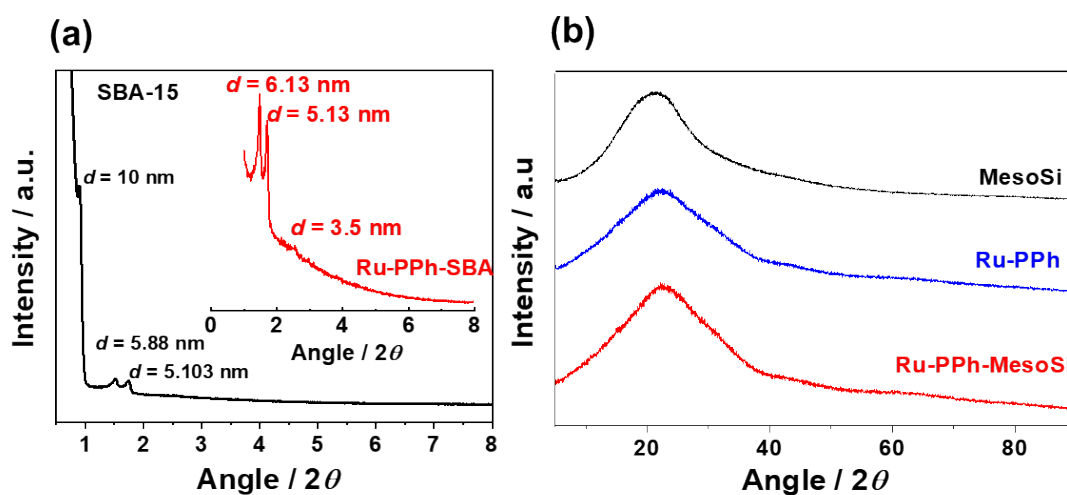


Fig. S2. (a) XRD of SBA-15 in black and SBA-15 templated Ru-PPh-SBA in red; (b) Wide-angle X-ray diffraction (WAXS) of template-free MesoSi (black); Ru-PPh (blue) and Ru-PPh-MesoSi (red)

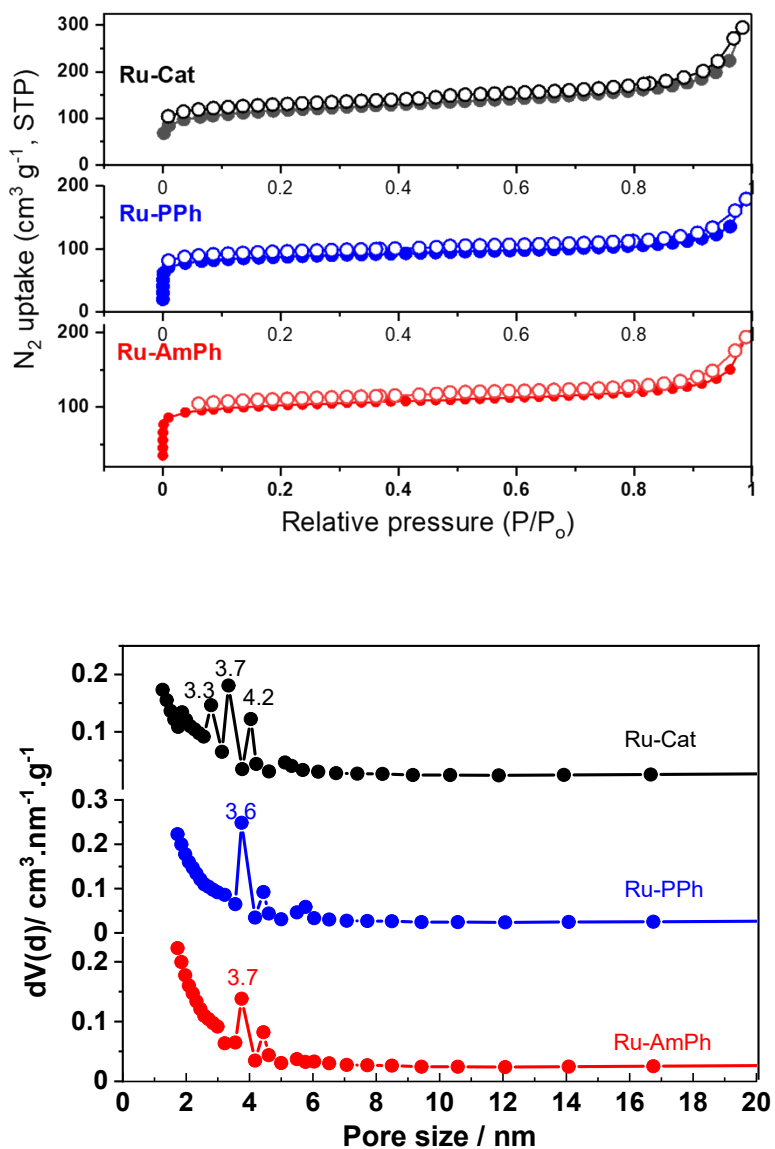


Fig. S3. (Top) N_2 sorption adsorption (closed) and desorption (open) isotherm of microporous Ru-catalysts synthesized without using silica templates; (Bottom) Pore size distribution; black (Ru-Cat); blue (Ru-PPh); red (Ru-AmPh)

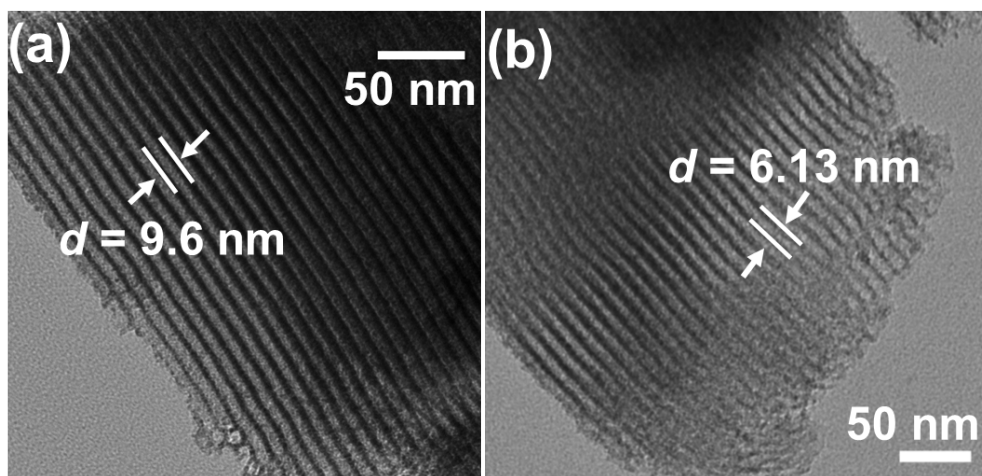


Fig. S4. HR-TEM of (a) SBA-15; (b) Ru-PPh-SBA

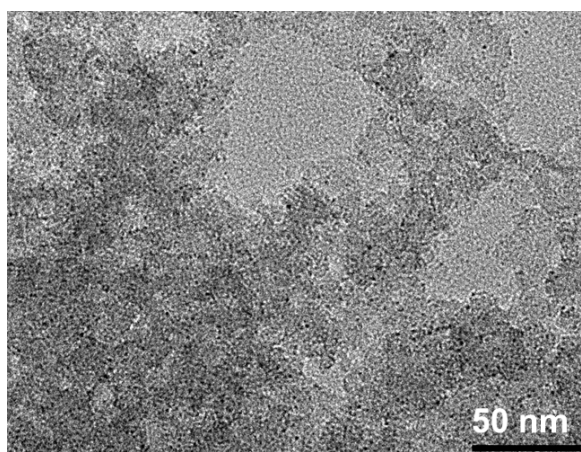


Fig. S5. HR-TEM image of microporous Ru-PPh, synthesized in absence of any hard templating approach.

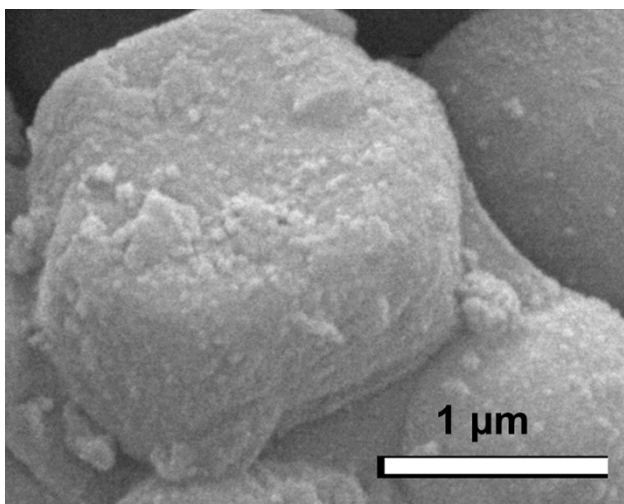


Fig. S6. Magnified FESEM image of template free mesoporous MesoSi

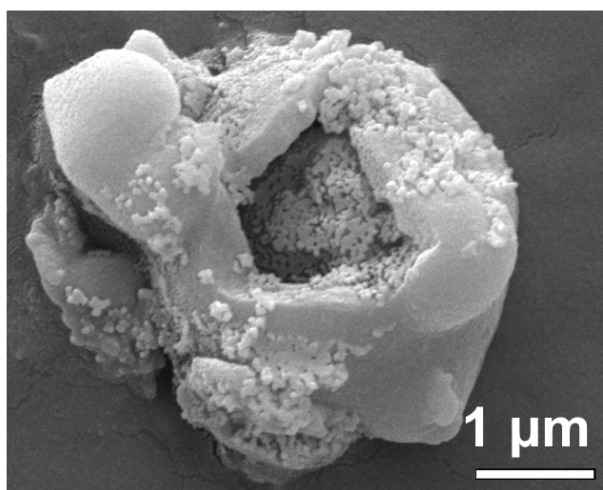


Fig. S7. FESEM image of template extracted PPh-SBA

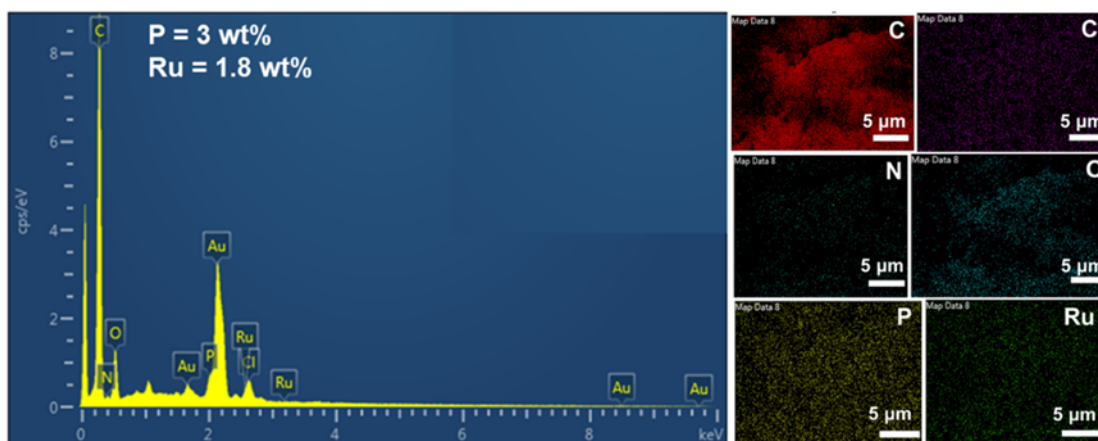


Fig. S8. FE-SEM EDX and elemental mapping of Ru-PPh-MesoSi

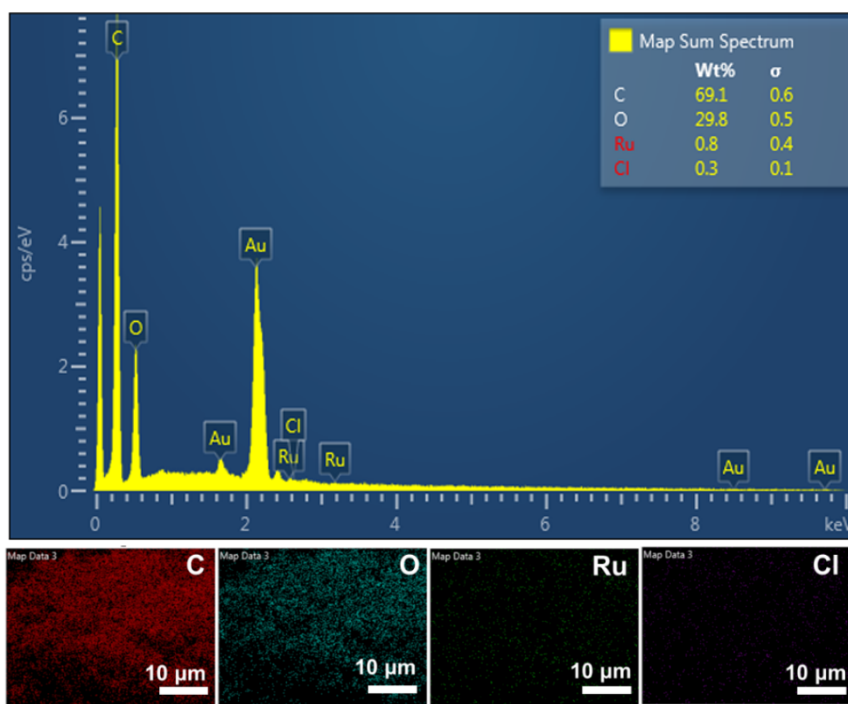


Fig. S9. FE-SEM EDX and elemental mapping of pristine Ru-Cat

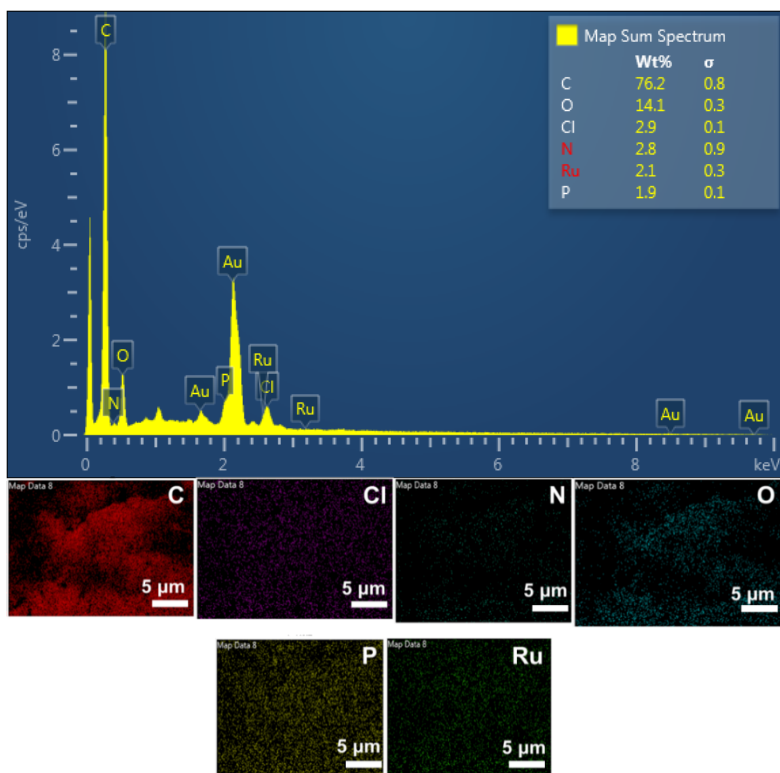


Fig. S10 FE-SEM EDX and elemental mapping of pristine Ru-AmPh

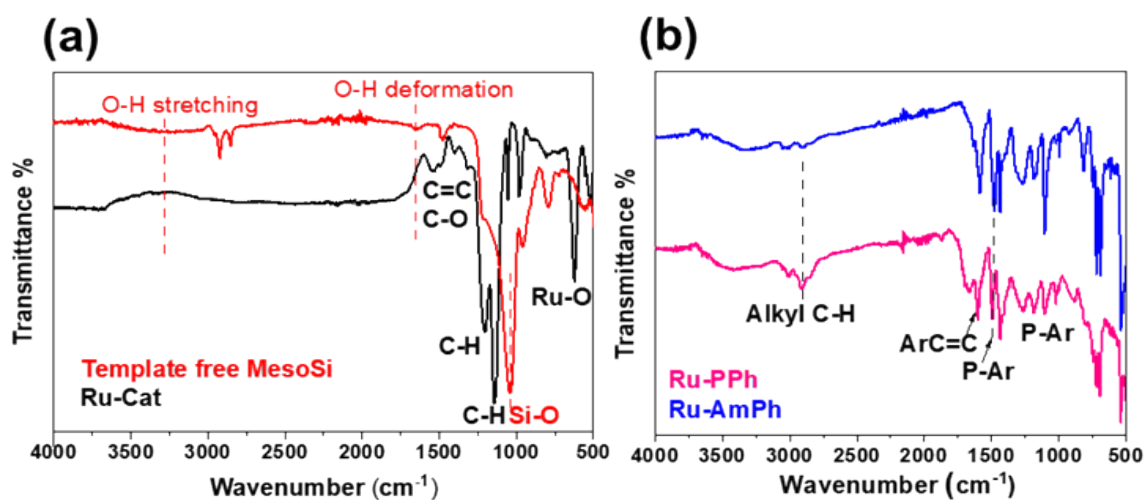


Fig. S11. FT-IR spectra of (a) template-free MesoSi, Ru-Cat, and (b) Ru-PPh and Ru-AmPh

EXAFS data collection and analysis results

Extended X-ray Absorption Fine Structure (EXAFS) measurements have been carried out at the Energy-Scanning EXAFS beamline (BL-9) at the Indus-2 Synchrotron Source (2.5 GeV, 100 mA) at Raja Ramanna Centre for Advanced Technology (RRCAT), Indore, India.^{8,9} This beamline operates in the energy range of 4 KeV to 25 KeV. The beamline optics consists of a Rh/Pt coated collimating meridional cylindrical mirror and the collimated beam reflected by the mirror is monochromatized by a Si(111) ($2d=6.2709 \text{ \AA}$) based double crystal monochromator (DCM). The second crystal of DCM is a sagittal cylinder used for horizontal focusing while an Rh/Pt coated bendable post mirror facing down is used for vertical focusing of the beam at the sample position. Rejection of the higher harmonics content in the X-ray beam is performed by detuning the second crystal of DCM. In this beamline, EXAFS measurements can be performed in both transmission and fluorescent mode.

In the present case, the measurements have been carried out in fluorescence mode where the sample is placed at 45° to the incident X-ray beam, and a fluorescence detector is placed at a right angle to the incident X-ray beam to collect the signal. One ionization chamber detector is placed before the sample to measure the incident flux (I_0) and fluorescence detector measures the fluorescence intensity (I_f). In this case, the X-ray absorption coefficient of the sample is determined by $\mu = I_f / I_0$, and the spectrum was obtained as a function of energy by scanning the monochromator over the specified range.

The normalized EXAFS ($\mu(E)$ vs. E) spectra of the samples at Ru Edge are shown in Figures 1. To obtain qualitative information about the local structure, oscillations in the absorption spectra $\mu(E)$ vs. E has been converted to absorption function $\chi(E)$ defined as follows⁹:

$$\chi(E) = \frac{\mu(E) - \mu_0(E)}{\Delta\mu_0(E_0)} \quad (5)$$

where E_0 is absorption edge energy, $\mu_0(E_0)$ is the bare atom background, and $\Delta\mu_0(E_0)$ is the step in value at the absorption edge. The energy-dependent absorption coefficient $\chi(E)$ has been converted to the wavenumber dependent absorption coefficient $\chi(k)$ using the relation,

$$K = \sqrt{\frac{2m(E - E_0)}{h^2}} \quad (6)$$

where m is the electron mass. $\chi(k)$ is weighted by k^2 to amplify the oscillation at high k and the $\chi(k)k^2$ functions are Fourier transformed in R space to generate the $\chi(R)$ versus R plots in terms of the real distances from the center of the absorbing atom. The Fourier transformed EXAFS spectra or $\chi(R)$ versus R plots of all the samples are shown in figures 2(a-c), where a k window of $2-10\text{\AA}^{-1}$, $3-10\text{\AA}^{-1}$, $2-8\text{\AA}^{-1}$ for Ru-Nh, Ru-meso, and Ru-PPh respectively has been used for Fourier transform for different samples depending on the useful data quality.

Theoretical $\chi(R)$ versus R plots have subsequently been generated using the standard EXAFS equation⁹ and using the basic crystallographic information of the samples and the theoretical plots have been fitted with the experimental data. During fitting, bond distances (R), co-ordination numbers (N) and disorder (Debye-Waller) factors (σ^2), which give the mean square fluctuations in the distances, have been used as fitting parameters. The goodness of fit has been determined by the value of the R_{factor} defined by:

$$R_{factor} = \sum \frac{[\text{Im}(\chi_{dat}(r_i) - \chi_{th}(r_i))]^2 + [\text{Re}(\chi_{dat}(r_i) - \chi_{th}(r_i))]^2}{[\text{Im}(\chi_{dat}(r_i))]^2 + [\text{Re}(\chi_{dat}(r_i))]^2} \quad (7)$$

where, χ_{dat} and χ_{th} refer to the experimental and theoretical $\chi(r)$ values respectively and Im and Re refer to the imaginary and real parts of the respective quantities. The fitting has been done upto the 1st major peak and the best-fit parameters for the samples have been shown in Tables-1, 2, and 3.

The set of EXAFS data analysis programmes available within the Demeter ¹⁰ software package has been used for EXAFS data analysis. This includes background reduction and Fourier transforms to derive the $\chi(R)$ versus R plots from the absorption spectra (using ATHENA code), generation of the theoretical EXAFS spectra starting from an assumed crystallographic structure and finally fitting of experimental data with the theoretical spectra using ARTEMIS code.

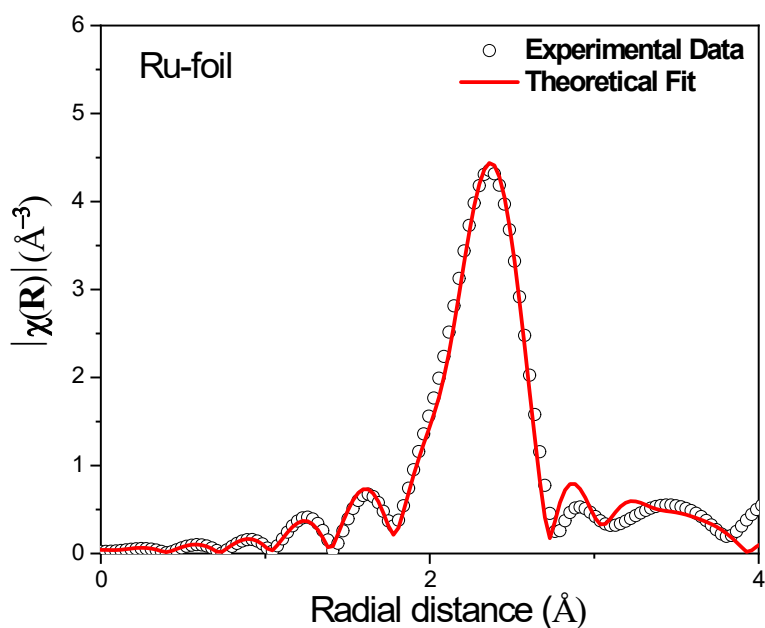


Fig. S12. Fourier transformed EXAFS spectra of Ru-Foil measured at Ru edge

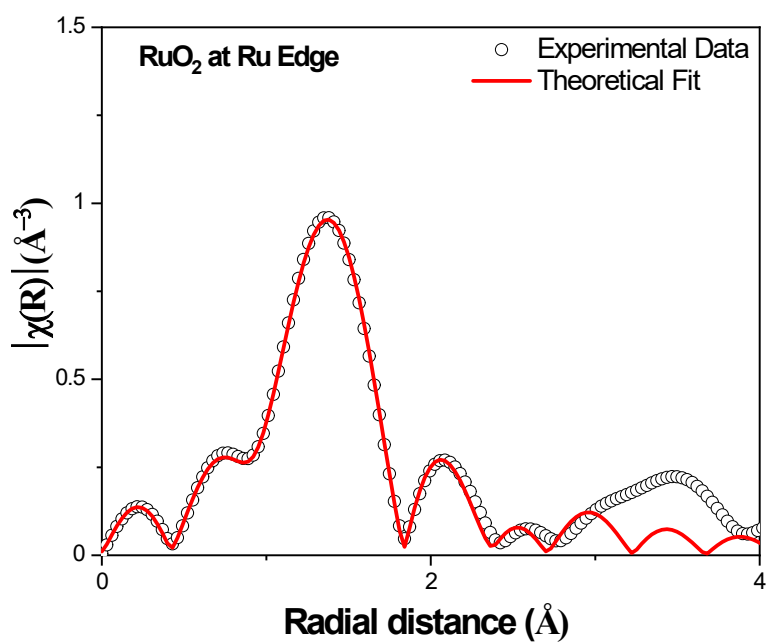


Fig. S13. Fourier transformed EXAFS spectra of RuO₂ measured at Ru edge

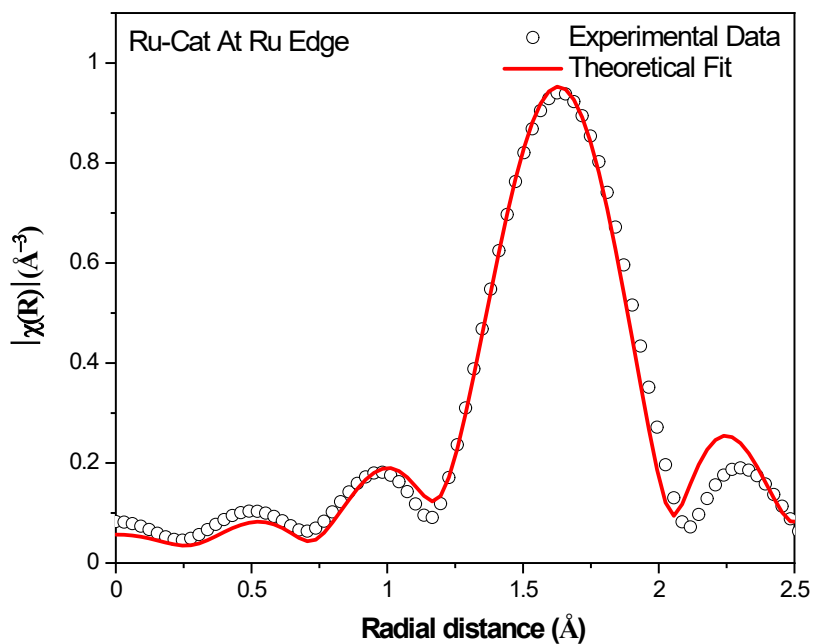


Fig. S14. Fourier transformed EXAFS spectra of Ru-Cat measured at Ru edge

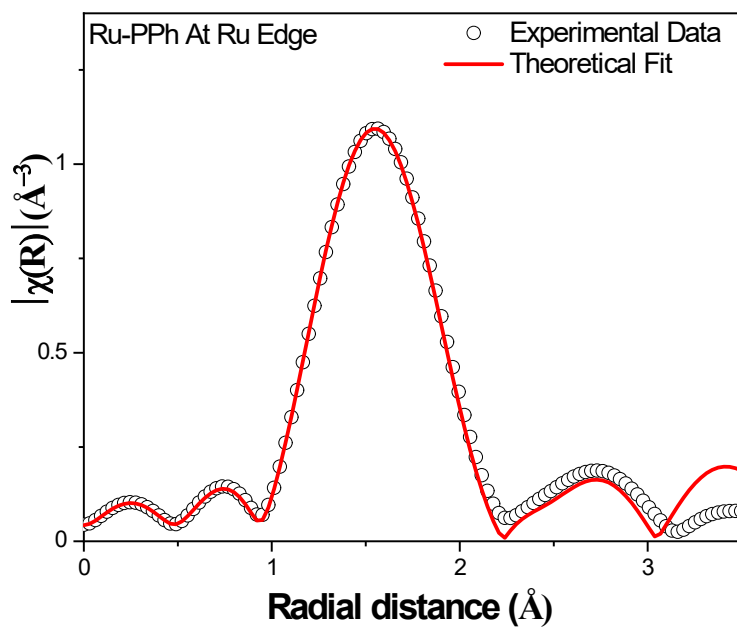


Fig. S15. Fourier transformed EXAFS spectra of Ru-PPh measured at Ru edge

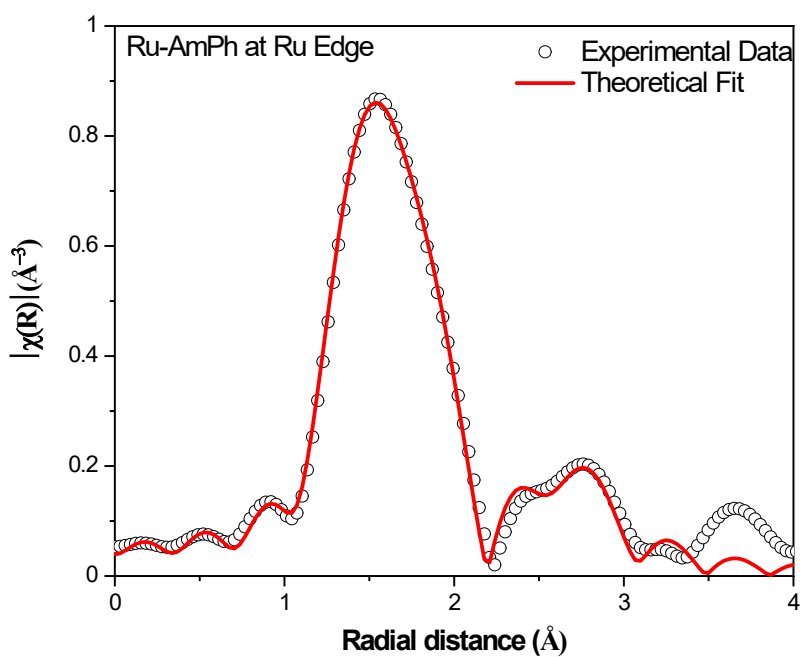


Fig. S16. Fourier transformed EXAFS spectra of Ru-AmPh measured at Ru edge

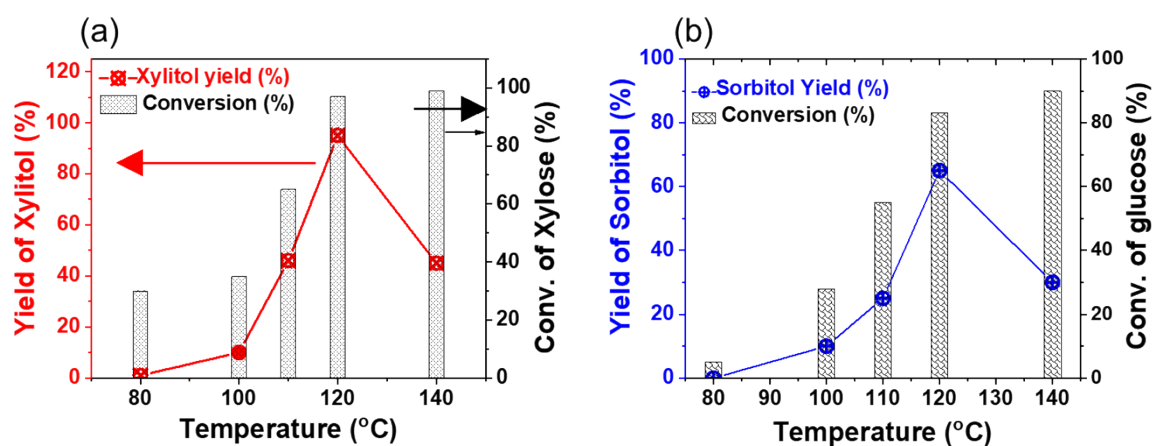


Fig. S17. Temperature effect on the hydrogenation of (a) xylose and (b) glucose respectively; unless otherwise noted, 20 mg xylose, 10 mg Ru-PPh-MesoSi (1 wt% of Ru-sites), 2 mL ultrapure water were mixed with FA (122 μ L), TA (140 μ L) and heated at 120 $^{\circ}$ C for 2 h in a microwave reactor

HPLC chromatograms of standards and the reaction mixture of the optimized reaction (Mobile phase: 5 mM H₂SO₄)

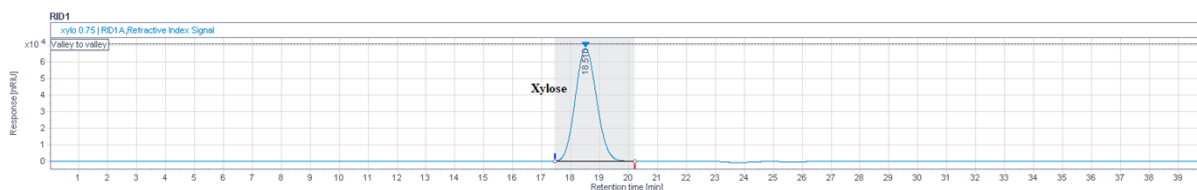


Fig. S18. HPLC chromatogram of standard Xylose, retention time: $t=18$ min.

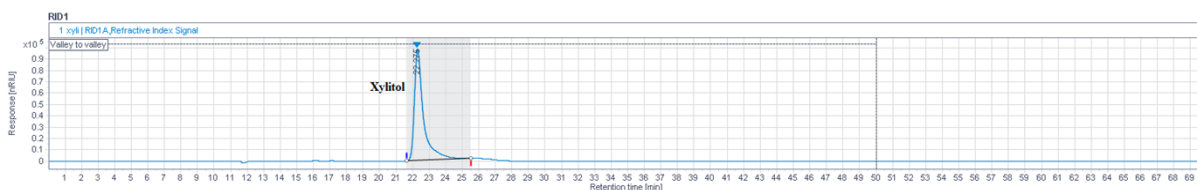


Fig. S19. HPLC chromatogram of standard Xylitol, retention time: $t=23$ min.

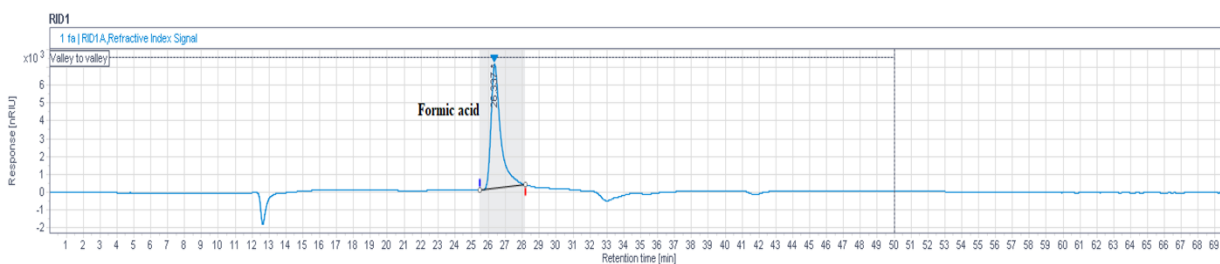


Fig. S20. HPLC chromatogram of standard Formic acid, retention time: $t=27$ min.

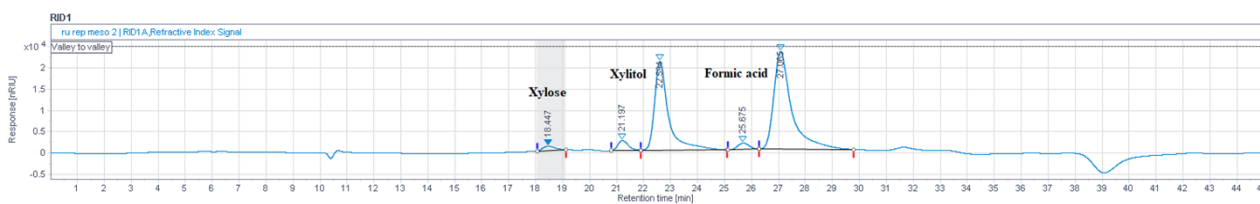


Fig. S21. HPLC chromatogram of the xylose hydrogenation reaction

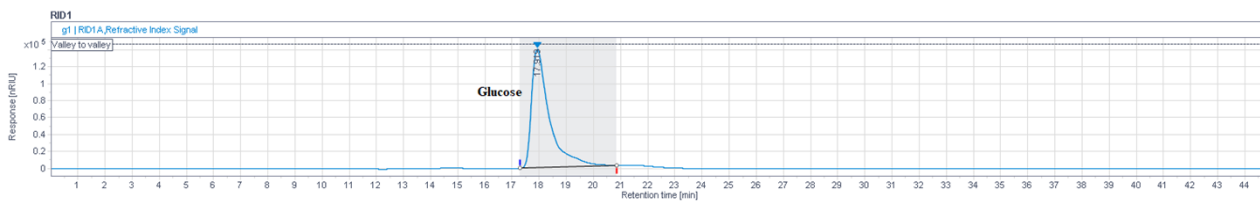


Fig. S22. HPLC chromatogram of standard glucose in water, retention time: 18 min

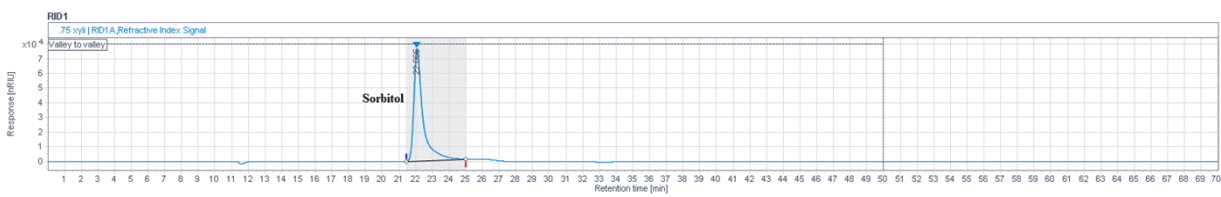


Fig. S23. HPLC chromatogram of standard sorbitol in water, retention time: 23 min

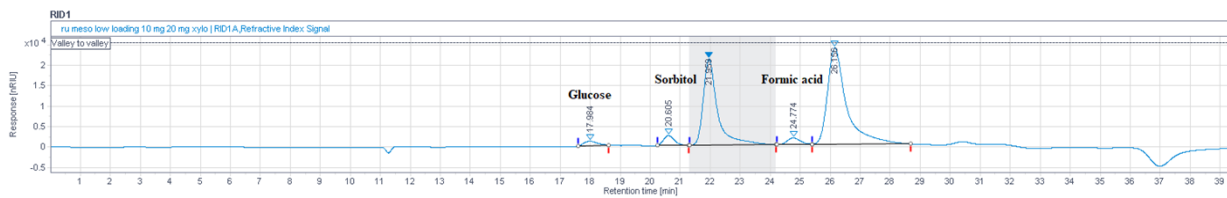


Fig. S24. HPLC chromatogram of the glucose hydrogenation reaction

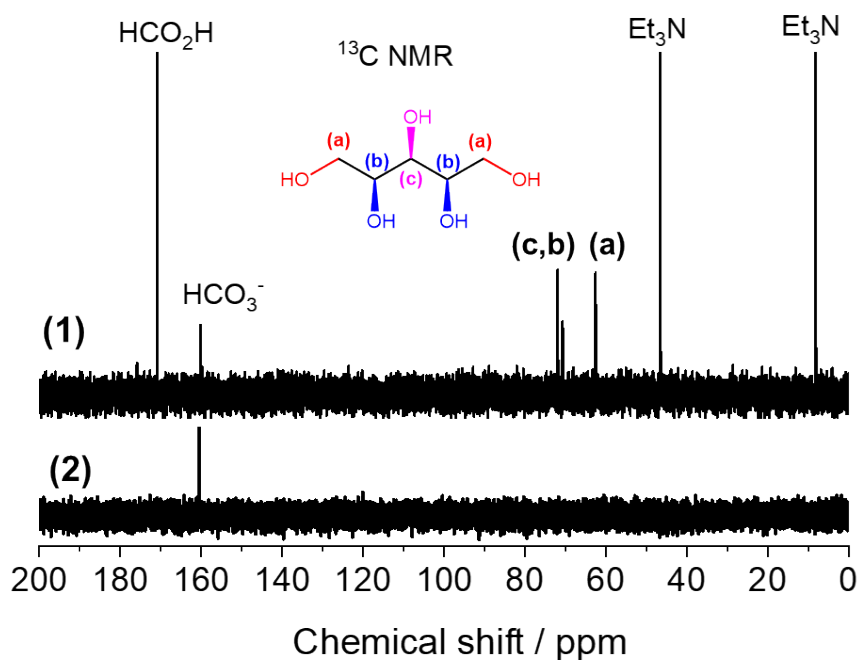


Fig. S25. (a) ^{13}C NMR of the reaction solution (D_2O) showing xylitol as the product from transfer hydrogenation of xylose using formic acid/trimethylamine; (b) ^{13}C NMR of standard sodium bicarbonate

Cohesive energy of bulk Ru and interaction energy of Ru with ligands

To check the stability of the single Ru-atom surrounded by different ligands. Here, we have calculated the cohesive energy of bulk Ru and the interaction energy of Ru with ligands. In bulk, Ru exists in a stable hexagonal phase (i.e., space group P63/mmc. To compute the cohesive energy of bulk we have used following equation Eq. 8:

$$E(\text{cohesive}) = E(\text{bulk}) - nE(\text{atom}) \quad (8)$$

$$E(\text{cohesive}) = E(\text{bulk}) - nE(\text{atom})$$

where, $E(\text{cohesive})$, $E(\text{bulk})$ and $E(\text{atom})$ stand for the cohesive energy, energy of bulk system and energy of single atom in the lattice, respectively. n is the number of the atoms in the bulk. We have observed that the cohesive energy of bulk Ru is positive i.e., 0.72 eV, whereas the interaction energy of Ru-atom with triphenylphosphine, triphenylamine and catechol are -1.36, -2.26 and -0.688 eV, respectively. As the interaction energy of Ru with the ligands is negative, this shows that single R-atom can be synthesized when it is surrounded by the polymers.

Energy profile for hydrogenation of the xylose to xylitol, using NEB approach

We have done NEB for xylose adsorption and partial hydrogenation of carbonyl group over the Ru single atom surrounded by the triphenylphosphine ligands (the most promising catalyst i.e., Ru-PPh-MesoSi). In Fig. S26, from ist initial state (SI) to iiird transition state (TS) the distance between the oxygen of the carbonyl group of xylose and the Ru atom decreases. At TS reaction step the H initially bonded with Ru atom interacts with the carbonyl group and in the ivth reaction step this H makes bond with C atom of the carbonyl group of the xylose and O atom is bonded with the Ru atom. In vth reaction step i.e., final state (FS) the bond length of Ru and O atom decreases, and this configuration is of minimum energy. Here, in Fig. S26, partial hydrogenation of the xylose has been shown from ist reaction step to the vth reaction step. Further, in Fig. S27, we have shown reaction steps for the complete hydrogenation of xylose and desorption of the xylitol from the Ru atom. In Fig. S27, in first reaction step (i), the H⁺ ion from the formic acid and NEt₃ system¹¹⁻¹³ interacts with oxygen adsorbed on the Ru atom. In step ii, oxygen atom makes bound with H⁺ ion and its bond with Ru atom becomes weak. In step iii the bond length of O and Ru atom increases, this shows that Ru-O bond is breaking. Here, steps ii and iii show the desorption of xylitol from

the Ru atom. Also, from the energies of the i, ii and iii reaction steps, we conclude that after complete hydrogenation of xylose to xylitol desorption is energetically favorable reaction.

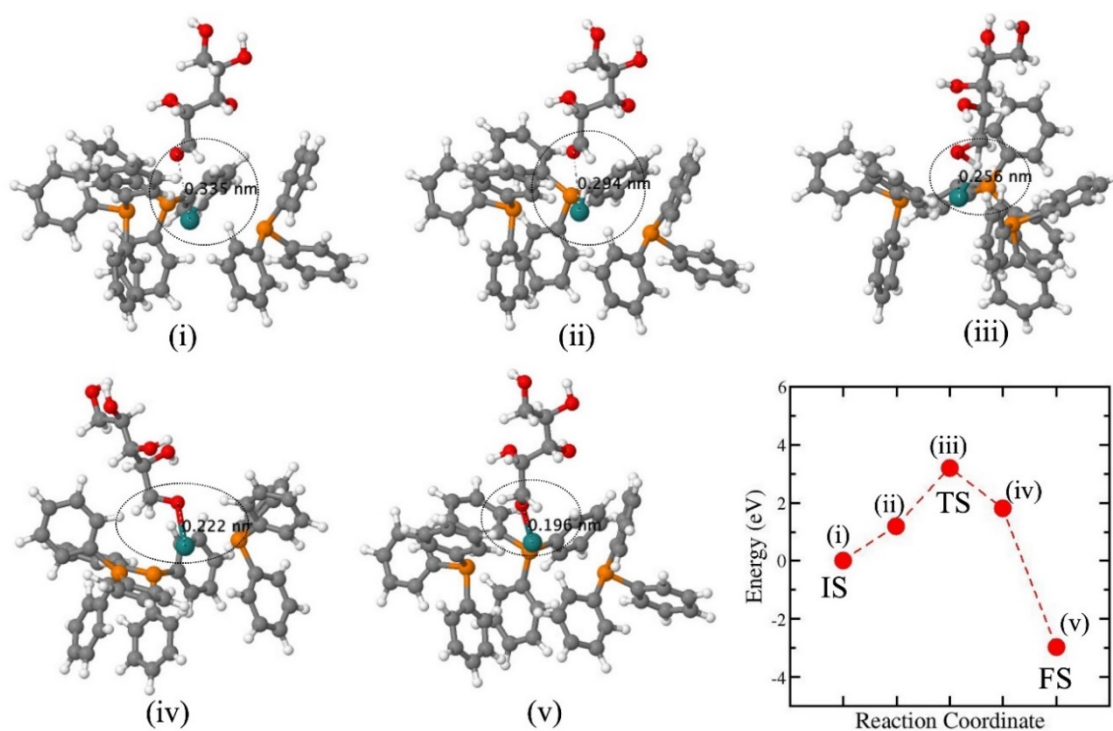


Fig. S26. Reaction profile for the adsorption and partial hydrogenation of the carbonyl group of the xylose with initial state (SI), transition state (TS) and final state (FS) on the single Ru atom surrounded by triphenylphosphine (Ru-PPh-MesoSi).

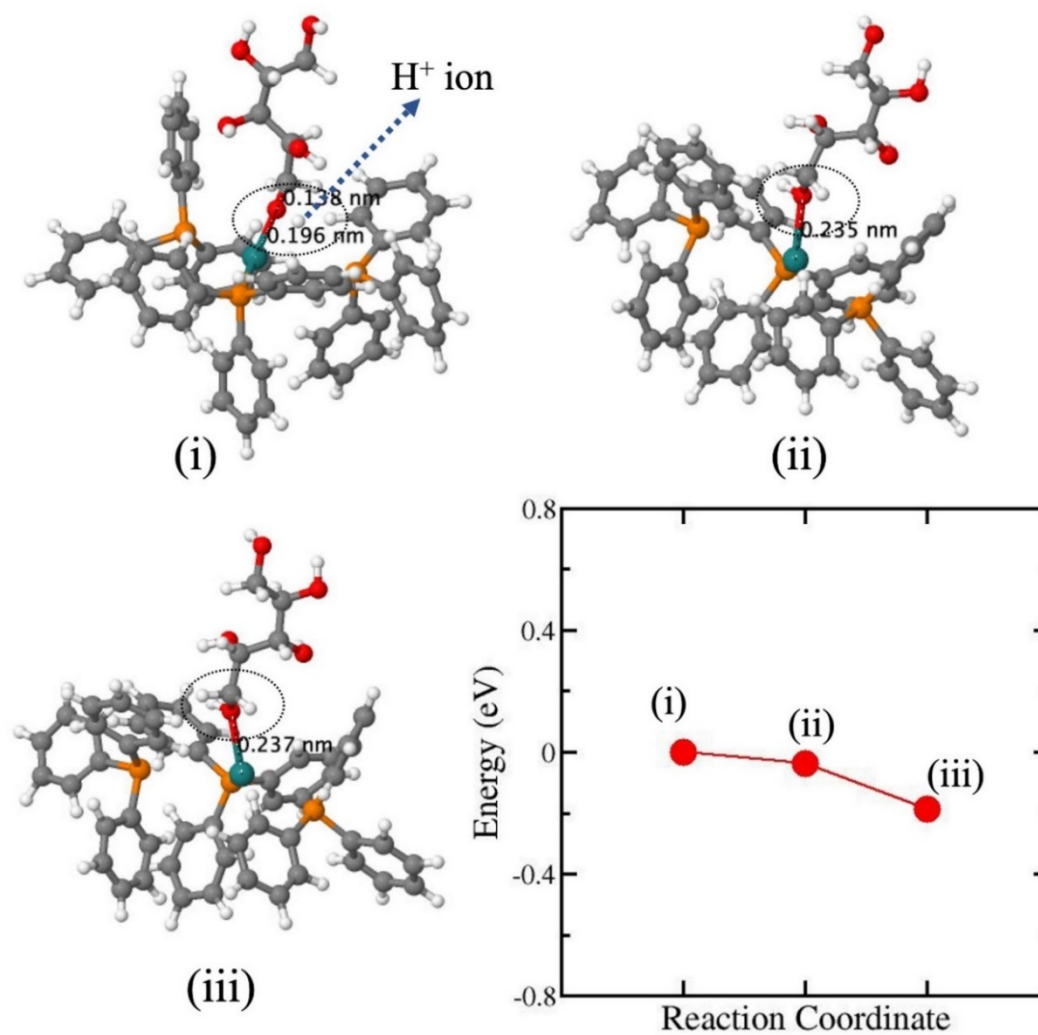


Fig. S27. Reaction profile for the desorption of xylitol from the single Ru atom surrounded by triphenylphosphine (Ru-PPh-MesoSi).

References

- 1 A. Modak, P. Bhanja and A. Bhaumik, *Chemistry - A European Journal*, 2018, **24**, 14189–14197.
- 2 P. Verma, Y. Kuwahara, K. Mori, R. Raja and H. Yamashita, *Functionalized mesoporous SBA-15 silica: Recent trends and catalytic applications*, Royal Society of Chemistry, 2020, vol. 12.
- 3 W. Stober and A. Fink, *J Colloid Interface Sci*, 1968, **26**, 62–69.
- 4 S. L. Suib, *Chemical Record*, 2017, **17**, 1169–1183.
- 5 W. Kohn, *Physical Review*, 1965, **140**, A1133.

- 6 P. Hohenberg and W. Kohn, *Physical Review*, 1964, **136**, B864.
- 7 J. P. Perdew, K. Burke and M. Ernzerhof, *Phys Rev Lett*, 1996, **77**, 3865–3868.
- 8 S. Basu, C. Nayak, A. K. Yadav, A. Agrawal, A. K. Poswal, D. Bhattacharyya, S. N. Jha and N. K. Sahoo, in *Journal of Physics: Conference Series*, Institute of Physics Publishing, 2014, vol. 493.
- 9 A. K. Poswal, A. Agrawal, A. K. Yadav, C. Nayak, S. Basu, S. R. Kane, C. K. Garg, D. Bhattacharyya, S. N. Jha and N. K. Sahoo, 2014, pp. 649–651.
- 10 B. Ravel and M. Newville, *J Synchrotron Radiat*, 2005, **12**, 537–541.
- 11 Q. Y. Bi, X. L. Du, Y. M. Liu, Y. Cao, H. Y. He and K. N. Fan, *J Am Chem Soc*, 2012, **134**, 8926–8933.
- 12 Q. T. Trinh, B. K. Chethana and S. H. Mushrif, *Journal of Physical Chemistry C*, 2015, **119**, 17137–17145.
- 13 P. N. Amaniampong, Q. T. Trinh, K. de Oliveira Vigier, D. Q. Dao, N. H. Tran, Y. Wang, M. P. Sherburne and F. Jérôme, *J Am Chem Soc*, 2019, **141**, 14772–14779.